Journal of Alloys and Compounds 509 (2011) 3613–3616

Contents lists available at ScienceDirect

Journal of Alloys and Compounds

journal homepage: www.elsevier.com/locate/jallcom

Size dependent luminescence of nanocrystalline Y_2O_3:Eu and connection to temperature stimulus

Zhang Wei-Wei[a,*], Yin Min[b], He Xing-Dao[a], Gao Yi-Qing[a]

[a] Aeronautic Science Key Laboratory for Aeronautic Testing and Evaluation, Nanchang Hangkong University, 330063 Nanchang, PR China
[b] Department of Physics, University of Science and Technology of China, 230026 Hefei, PR China

ARTICLE INFO

Article history:
Received 11 September 2010
Received in revised form
12 December 2010
Accepted 15 December 2010
Available online 23 December 2010

Keywords:
Nanostructured materials
Luminescence
Size effect
Temperature dependence

ABSTRACT

In the emission spectra of nanocrystalline Y_2O_3:Eu with decreasing the particle size, the $^5D_0$–$^7F_0$ transition of Eu^{3+} shifts towards blue. This size effect is explained by lattice expansion of the nanocrystallines, more precisely, by larger Eu–O distance. Meanwhile, increasing temperature also expands the lattice constant and shifts the emission peak to blue. Then nephelauxetic effect is employed to organize the size effect and temperature dependence. It is also introduced to indicate the change of Eu^{3+} coordination number in the nanosized phosphor. Based on the experimental results, possible applications of temperature sensing and stress mapping with Eu^{3+} doped nanocrystalline phosphors are proposed.

1. Introduction

Rare earth sesquioxide nanophosphors have received extensive attention due to their unique properties and potential applications in various fields, such as white LED phorphors [1], scintillation phosphors [2], upconversion phosphors [3,4], laser medium [5,6]. The latest developments include but are more than these: the influence of codoping various metal ions [7–9], the effect of surface modification on nanoparticles [10], the control of the nanocrystal shape via various synthesis methods [11–14]. Among the materials, Re_2O_3:Eu (Re = Y, Gd, Lu) are typical, as Eu^{3+} is hypersensitive to its configuration circumstance and plays the role of probe ion.

Eu^{3+} ions occupy sites with C_2 and C_{3i} symmetry in host lattice of cubic Re_2O_3, making Gd_2O_3:Eu, Y_2O_3:Eu, and Lu_2O_3:Eu similar in luminescent spectra feature [15]. The nanosized phosphors also present similar size dependence of luminescence [10,12–16], including novel $^5D_0 \rightarrow {}^7F_2$ emission band, shift of the charge transfer band (CTB), short fluorescence lifetime, and high quenching concentration. However, there is much controversy about (1) shift direction of CTB [15–19] and (2) blue shift of emission peaks [16,20,21]. Recent reports [17,18] have achieved a probably certain conclusion that, in nanosized Re_2O_3:Eu, CTB of surface Eu^{3+} has a red shift when that of interior Eu^{3+} moves towards blue. In fact, if the coordination parameters of Eu^{3+} are determined, CTB position can be calculated theoretically [15,22]. As for blue shift of emission peaks, the occupancy of Eu^{3+} into Y^{3+} sites seems to change the emission peak position [23]. Also C_2 to C_{3i} sublattice population was considered being influenced by nanosize [24].

In this paper, the relationship between photoluminescence and particle size of Y_2O_3:Eu is studied. Then based on the analysis of the change of Eu^{3+} coordination parameters, the relationship between transition energies of Eu^{3+} and lattice constant is deduced. Our study indicates that, both increasing temperature and decreasing particle size of Y_2O_3:Eu can expand the host lattice, and correspondingly show the same response of luminescent spectroscopies.

2. Experimental setup

Nanocrystalline Y_2O_3:Eu is synthesized by liquid combustion method [16,25]. The aqueous solutions of metal nitrates and glycin were dried and then heated to self-igniting, after they were mixed. The residual powders were the desired phosphors.

X-ray powder diffraction (XRD) measurements for the materials were carried out on MXP18AHF X-ray diffractometer from MAC science Co., Ltd. For luminescence measurement, the samples were excited with a frequency tripled YAG:Nd laser. A Jobin–Yvon HRD1 monochrometer was used to analyze the fluorescent spectra.

3. Results and discussion

Obtained products are in pure phase with a cubic structure (JCPDS No. 25-1200). From the well-known Scherrer equation, the particle sizes of nanocrystals were estimated by the full width at half magnitude (FWHM) of the XRD peaks (Fig. 1). The particle sizes of sample B, C, D, E are about 80 nm, 40 nm, 10 nm and

* Corresponding author. Tel.: +86 15170463677; fax: +86 791 3953461.
E-mail addresses: zdw@ustc.edu, zhangww74@yahoo.com.cn (Z. Wei-Wei).

0925-8388/$ – see front matter © 2010 Elsevier B.V. All rights reserved.
doi:10.1016/j.jallcom.2010.12.110

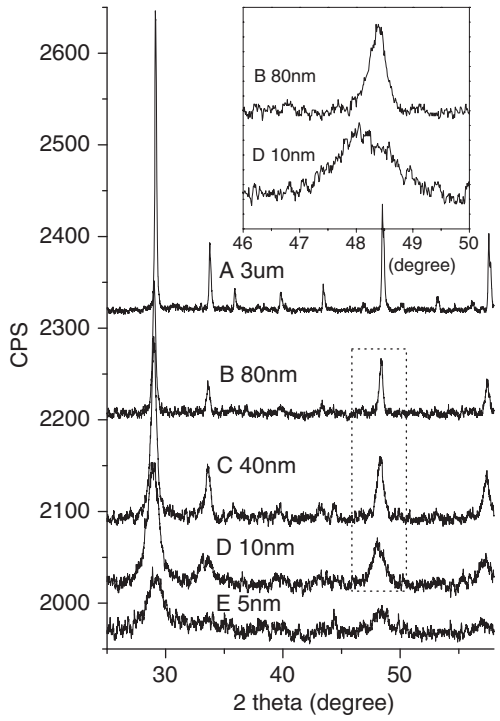

Fig. 1. XRD patterns of nanocrystalline Y_2O_3:Eu, at room temperature.

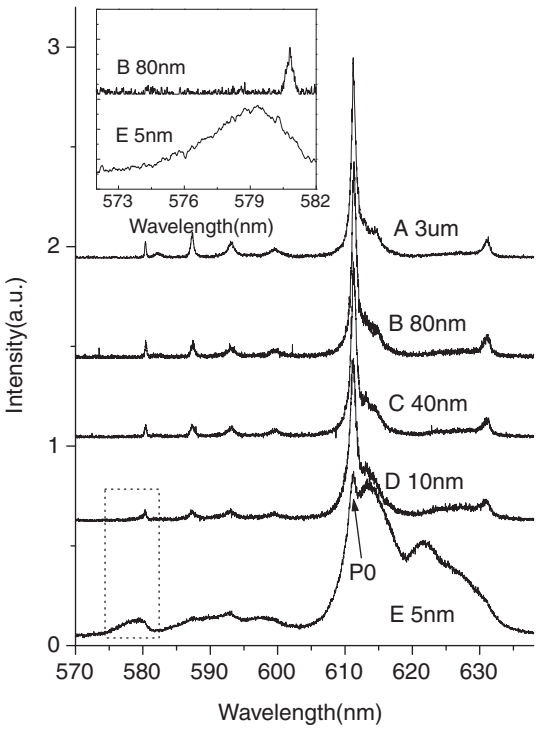

Fig. 2. Emission spectra of nanocrystalline Y_2O_3:Eu (inset: $^5D_0 \rightarrow {}^7F_0$ transition of Eu^{3+}) at room temperature, λ_{ex} = 355 nm.

5 nm respectively, while that of the commercial bulk Y_2O_3:Eu phosphor (sample A) is larger than 3 μm. Slight red shift of the XRD peaks (inset of Fig. 1) of the nanosized particles was noticed. Such a shift of XRD peak was also reported elsewhere [15,16]. Lattice constants with different particle sizes are calculated from the XRD patterns and shown in Table 1. Compared with the normal sized sample (sample A) which has a lattice constant 1.060 nm at room temperature, the nanocrystals always have lattice expansion. The smaller the particle size is, the larger the lattice constant is. Namely, lanthanide-ligand distance in nanocrystal depends on the particle size.

The lattice constant can also be affected by temperature and pressure through changing material volume. Coefficient of thermal expansion (CTE) of yittria is about 4.2–8.5 ppm/K, depending on temperature and bulk size [26,27]. Assuming that a linear shrinkage takes place when the nanosized phosphor is under lowering temperature, and the CTE is set as average value ~6.5 ppm/K, lattice constant at 10 K can be calculated and added into Table 1.

The photoluminescence of Y_2O_3:Eu (Fig. 2) is greatly affected by Eu^{3+} coordination circumstance. The sole weak peak of $^5D_0 \rightarrow {}^7F_0$ transition is from Eu^{3+} at C_2 site. A careful analysis on this peak shows blue shift with decreasing particle size (inset of Fig. 2). That is to say, energy level of $^5D_0$ moves upward in a small particle sized sample with respect to the $^7F_0$ level. As it is well known that, the crystal field of host affects the energy levels of a rare earth ion. Accordingly, the shifts can be related to the change of the host lattice. Similar effect was found in certain host crystal and doped ion. The lattice constant can be slightly changed with temperature, e.g. the transition of $^5D_0 \rightarrow {}^7F_0$ of Eu^{3+} in YBO_3:Eu shifts from 580.86 nm to 581.04 nm when the temperature drops from room temperature to 11 K [28]. Such a temperature dependent red shift of the level in normal sized YBO_3:Eu resulted from the decrease of the Eu–O bond length. The same tendency of shift is exhibited for the barycenter (also named 'center of mass') of the $^7F_2$ energy level (Table 1) in nanocrystalline Y_2O_3:Eu.

Above phenomena of shifts can be explained by nephelauxetic effect [29], which means the size of the electron cloud around the lanthanide ion increases due to transferring electron density to bonding molecular orbital. The increase of cloud size results in a decrease of the electrostatic repulsion. Nephelauxetic effect is essential for $4f^{n-1}5d$ electrons. ΔE(fd) is the barycenter energy of the $4f^{n-1}5d$ configuration above the barycentre energy of the $4f^n$ configuration. E_{avg} parameter for $4f^n$ configuration represents the barycentre energy level of the configuration with respect to the ground state, while $E_{avg} + \Delta E$(fd) represents the barycenter energy of the excited configuration above ground state – a quantity hard to determine. Lowest energy state of excited configuration is well determined from experiment. Therefore once the other parameters are determined, the energy parameter ΔE(fd) is adjusted so that

Table 1
The lattice constants and level positions of nanocrystalline Y_2O_3:Eu.

Sample	B	C	D	E
Particle size (nm)	80	40	10	5
Lattice contant (nm, @RT)	1.06359 ± 0.00002	1.06459 ± 0.00002	1.06678 ± 0.00005	1.06857 ± 0.00007
[a]Lattice contant (nm, @10 K)	1.06159	1.06258	1.06477	1.06656
$^5D_0$ position (cm^{-1}, @10 K)	17,217	17,219	17,222	17,262
$^5D_0$ position (cm^{-1}, @RT)	17,229	17,229	17,232	17,265
$^7F_2$ barycenter (cm^{-1}, @10K)	959.4	970.4	988.5	1089.7
$^7F_2$ barycenter (cm^{-1}, @RT)	984.5	990.6	1003.6	1088.9

[a] Values are calculated from lattice constant at room temperature when assuming a linear coefficient of thermal expansion ~6.5 ppm/K.

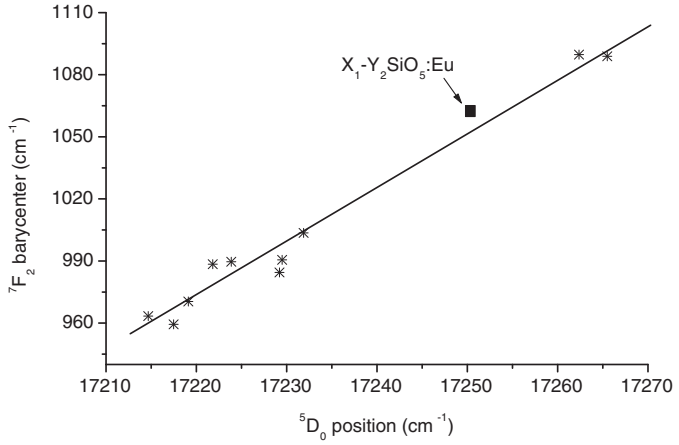

Fig. 3. The wavenumbers of the $^7F_2$ level barycenter as a function of those of the $^5D_0$ level for nanocrystalline Y_2O_3:Eu.

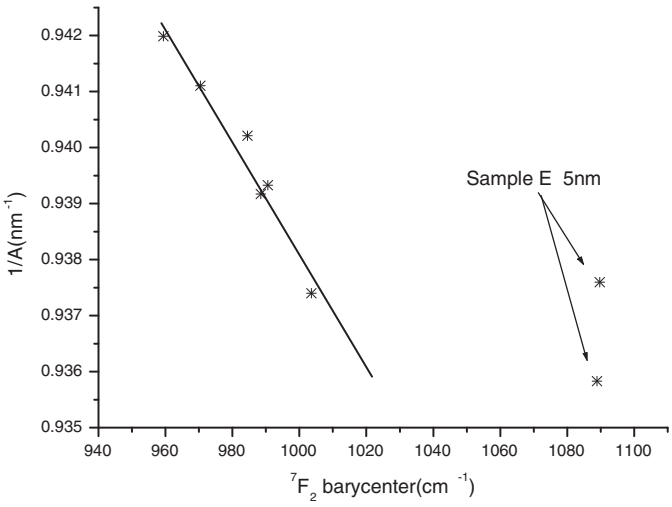

Fig. 4. The inverse of lattice constant as a function of the $^7F_2$ level barycenter for nanocrystalline Y_2O_3:Eu.

calculated and experimental values match for the lowest configuration energy level [30]. As for $4f^n$–$4f^n$ transition, a linear relation between barycenter energy levels has been reported [31].

According to the theory and experimental conclusion of nephelauxetic effect [29–31], the relationship between $^5D_0$ position and $^7F_2$ barycenter of Eu^{3+} in nanocrystalline Y_2O_3 can be fitted with a linear function. Fig. 3 shows the evolution of the energy level barycenter of Y_2O_3:Eu. Mixed data plotted here were all from nanocrystalline/bulk Y_2O_3:Eu samples with different particle sizes and/or at different temperatures. As what E. Antic-Fidancev has got from multiple hosts [31], the dependence from the mere Y_2O_3:Eu has also a linear slope. To test the validity, the result of Eu^{3+} in site 2 of X_1–Y_2SiO_5:Eu at 10 K [32] was also plotted in the figure (marked ■). The consistency for the two kinds of samples greatly supports the validity of aforementioned linear function. Hence the linear slope concludes size dependent peak shifts. Eu–O distance is the impact factor when coordination number of Eu^{3+} is constant.

An early question about the factor determining the $^5D_0$ level position of Eu^{3+} in nanocrystalline Y_2O_3 [33] has been answered herein. Taking a look at the size dependent movement of $^5D_0$, $^7F_1$ and $^7F_2$ energy levels, one can find an almost constant 'delta' between the levels. The energy levels move towards the same direction, making a nearly constant level gap. In other words, almost the same emission wavelengths were observed. Emission peaks of $^5D_0 \rightarrow {}^7F_{1,2}$ of nanocrystalline Y_2O_3:Eu always appear at the same positions as bulk phosphor. The results in seemingly non-shift peaks are consistent with other reports [20,21].

Besides the blue shift of emission peaks, another size effect of nanocrystalline Y_2O_3:Eu is the odd spectrum feature of sample E (Fig. 2). Emission of sample E is quite different with others, even that the $^5D_0 \rightarrow {}^7F_2$ transition of Eu^{3+} (600–640 nm) still dominates the emission spectrum. The emission band mainly consists of a sharp peak at 611 nm (P0) and two wide bands in the region of 612–630 nm. Different feature implies a changing environment of Eu^{3+}. The coordination parameters of Eu^{3+} include site symmetry, coordination number and metal–legand distance. It has been displayed in Table 1 that metal–legand distances are different in the samples. However, if the coordination number and site symmetry remain the same, there will be the same transition selection rules and similar transition probability. Hence, the emission of sample E must indicate the change of coordination number or site symmetry of Eu^{3+}. Normally, there are more defects – e.g. lattice distortion – in nanocrystal than in bulk material. Namely site symmetry of Eu^{3+} in sample E is lower than the one in other samples. That must be one of the origins of new emission bands. The following analysis suggests another origin – changed coordination number, which will be more important.

Coordination parameters are the parameters for nephelauxetic effect. The effect can be theoretically derived from point-charge model. The Hamiltonian of crystal field is set as a perturbation to the Hamiltonian of a free ion. A 0th-term of the crystal field Hamiltonian is suggested to be in charge of the nephelauxetic effect. When an effective ionization degree of metal–ligand bond is considered constant in certain materials, the nephelauxetic effect is determined by structural characteristics, namely lanthanide–ligand distance R and the coordination number M. Here in this case, the distance R of Eu–O is proportional to lattice constant A. If M is constant, the $^7F_2$ barycenter will linearly depend on A^{-1}. The corresponding result shown in Fig. 4 indicates that, all Y_2O_3:Eu samples follow the linear dependence except sample E. For this departure from linearity, either the coordination number of Eu^{3+} in this sample E is not six, or wrong coefficient of thermal expansion was assigned to the sample. Since sample E at room temperature does not conform to the linear rule, we can conclude that, coordination number of Eu^{3+} in sample E is not six but larger. Larger coordination number and shrinked lattice constant drive the energy shift towards same direction. That explains why the two data points from sample E are above the fitting line in Fig. 4. EXAFS experiment has also proved that the changed coordination number is eight instead of six [34].

As the coordination number of Eu^{3+} changes, the site symmetry should also be modified. Asymmetry ratio is an indicator of the average coordination polyhedron of the Eu^{3+} ion. It is defined as the intensity ratio $I(^5D_0–{}^7F_2)/I(^5D_0–{}^7F_1)$ [35]. Calculated asymmetry ratio of sample A is 5.1. It varies to 6.7 in sample E, indicating much lower local symmetry of Eu^{3+}.

4. Further applications

Environmental parameters – both temperature and pressure – can affect the lattice constant of crystal, and then change the crystalline field. Following the aforementioned analysis, some applications of the relationship between transition energies (or emission wavelength) and lattice constant can be expected.

Based on the present experimental results, one possible application is temperature sensor. In a narrow temperature changing range, barycenter of energy level $^5D_0$ of Eu^{3+} vs. inverse of temperature can have a linear slope, as shown in Fig. 5. The relationship between barycenter of energy level and temperature is a monotonic function. Hence, the barycenter position can be used to sense temperature. This proposed technology eliminates the influence of

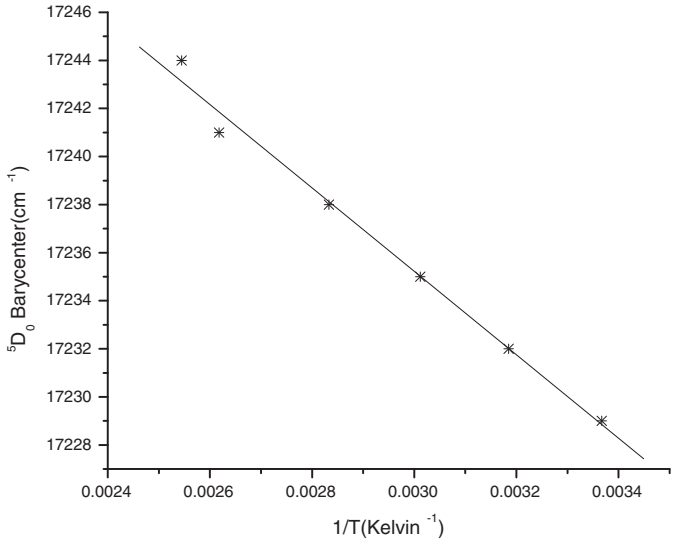

Fig. 5. The $^5D_0$ level barycenter as a function of temperature for nanocrystalline Y_2O_3:Eu, with particle size 80 nm.

fluctuation of absolute luminescent intensity, and is related to the contour of luminescent spectra only. So, we may expect the same precision of this method as that of Fluorescence Intensity Ratio (FIR) technology [36,37]. The proposed temperature sensing mechanism must be attractive for applications in EMI circumstance.

Another potential application is stress mapping. Similar technology elsewhere is known as fluorescent piezo-spectroscopic effect [38–40], which is based on the stress induced shift of R1 and/or R2 lines of Cr^{3+} in alumina. In this article, the possibility of Eu^{3+} as piezo-spectroscopic ion is introduced. One advantage of nanocrystalline Y_2O_3:Eu for stress mapping is highly sensitive. Assuming that the elastic modulus of sample D is 100 GPa and ignoring the Poisson deformation, the inverse of lattice constant will change 0.001 nm^{-1} at 100 MPa stress. According to Fig. 4, corresponding shift of Eu^{3+} $^7F_2$ barycenter is ~10 cm^{-1}. By contrast, only ~0.4 cm^{-1} shift is made by 100 MPa stress with piezo-spectroscopy effect of Al_2O_3:Cr [40]. Lattice expansion enhances the strain sensitivity at the same stress level. The extremely high piezo-sensitivity of nanoscale phosphors makes them appealing active materials for stress and strain sensing.

5. Conclusions

In conclusion, it has been shown that blue shift of luminescent peaks of nanocrystalline Y_2O_3:Eu was caused by lattice expansion. The effect of lattice expansion in nanoscale materials plays the same role as that of thermal expansion. Hence, such lattice expansion of nanocrystalline Y_2O_3:Eu makes its luminescence more sensitive to temperature and stress. The origin of new emission bands of nanocrystalline Y_2O_3:Eu was also studied with nephelauxetic effect.

Acknowledgements

We are greatly indebted to the reviewers who kindly contributed to the manuscript review and offered very valuable suggestions.

This project is supported by Open Fund of Aeronautical Science and Technology Key Lab. of Aeronautical Test and Evaluation, AVIC.

References

[1] B. Umesha, B. Eraiah, H. Nagabhushana, B.M. Nagabhushana, G. Nagaraja, C. Shivakumara, R.P.S. Chakradhar, J. Alloys Compd. 509 (2011) 1146–1151.
[2] N.V. Babayevskaya, T.G. Deyneka, P.V. Mateychenko, N.A. Matveevskaya, A.V. Tolmachev, R.P. Yavetskiy, J. Alloys Compd. 507 (2010) L26–L31.
[3] F. Qin, Y. Zheng, Y. Yu, Z. Cheng, P.S. Tayebi, W. Cao, Z. Zhang, J. Alloys Compd. 509 (2011) 1115–1118.
[4] Q. Lü, Y. Wu, L. Ding, G. Zu, A. Li, Y. Zhao, H. Cui, J. Alloys Compd. 496 (2010) 488–493.
[5] K. Serivalsatit, B.Y. Kokuoz, B. Kokuoz, J. Ballato, Opt. Lett. 34 (2009) 1033–1035.
[6] D. Zhou, Y. Shi, P. Yun, J.J. Xie, J. Alloys Compd. 479 (2009) 870–874.
[7] M. Yang, Y. Sui, S. Wang, X. Wang, Y. Wang, S. Lü, Z. Zhang, Z. Liu, T. Lü, W. Liu, J. Alloys Compd. 509 (2010) 827–830.
[8] K.M. Nissamudeen, K.G. Gopchandran, J. Alloys Compd. 490 (2010) 399–406.
[9] X. Hou, S. Zhou, Y. Li, W. Li, J. Alloys Compd. 494 (2010) 382–385.
[10] H. Wei, Z. Cleary, S. Park, K. Senevirathne, H. Eilers, J. Alloys Compd. 500 (2010) 96–101.
[11] D. Zhang, T. Yan, L. Shi, H. Li, J.F. Chiang, J. Alloys Compd. 506 (2010) 446–455.
[12] S. Zhong, J. Chen, S. Wang, Q. Liu, Y. Wang, S. Wang, J. Alloys Compd. 493 (2010) 322–325.
[13] R. Srinivasan, N.R. Yogamalar, J. Elanchezhiyan, R.J. Joseyphus, A.C. Bose, J. Alloys Compd. 496 (2010) 472–477.
[14] R. Krsmanović, Ž. Antić, B. Bártová, M.D. Dramićanin, J. Alloys Compd. 505 (2010) 224–228.
[15] L. Li, H.K. Yang, B.K. Moon, B.C. Choi, J.H. Jeong, K.H. Kim, Mater. Chem. Phys. 119 (2010) 471–477.
[16] W.W. Zhang, W.P. Zhang, P.B. Xie, M. Yin, H.T. Chen, L. Jing, Y.S. Zhang, L.R. Lou, S.D. Xia, J. Colloid Interface Sci. 262 (2003) 588–593.
[17] M. Yang, Y. Sui, S. Wang, X. Wang, Y. Wang, S. Lü, T. Lü, W. Liu, J. Alloys Compd. 509 (2011) 266–270.
[18] Y. Li, J. Zhang, X. Zhang, Y. Luo, S. Lu, Z. Hao, X. Wang, J. Phys. Chem. C 113 (2009) 17705–17710.
[19] P.A. Tanner, L. Fu, B. Cheng, J. Phys. Chem. C 113 (2009) 10773–10779.
[20] X. Ye, W. Zhuang, Y. Hu, T. He, X. Huang, C. Liao, S. Zhong, Z. Xu, H. Nie, G. Deng, J. Appl. Phys. 105 (2009) 064302–064307.
[21] B.V. Hao, P.T. Huy, T.N. Khiem, N.T.T. Ngan, P.H. Duong, J. Phys.: Conf. Ser. 187 (2009) 012074.
[22] L. Li, S.Y. Zhang, J. Phys. Chem. B 110 (2006) 21438–21443.
[23] D. Singh, L.R. Singh, Ind. J. Eng. Mater. Sci. 16 (2009) 175–177.
[24] T. Minami, W. Wang, F. Iskandar, K. Okuyama, Jpn. J. Appl. Phys. 47 (2008) 7220–7223.
[25] M. Rekha, K. Laishram, R.K. Gupta, N. Malhan, A.K. Satsangi, J. Mater. Sci. 44 (2009) 4252–4257.
[26] B.M. Walsh, J.M. McMahon, W.C. Edwards, N.P. Barnes, R.W. Equall, R.L. Hutcheson, J. Opt. Soc. Am. B 19 (2002) 2893–2903.
[27] D.C. Harris, Materials for Infrared Windows and Domes: Properties and Performance, SPIE, 1999, p. 126.
[28] W.W. Zhang, P.B. Xie, W.P. Zhang, M. Yin, L. Jing, S.Z. Lu, L.R. Lou, S.D. Xia, Chin. J. Inorg. Mater. 16 (2001) 9–16.
[29] C. Görller-Walrand, K. Binnemans, Rationalization of crystal-field parametrization, in: K.A. Gschneidner Jr., L. Eyring (Eds.), Handbook on the Physics and Chemistry of Rare Earths, vol. 23, Elsevier Science, 1996, pp. 163–164.
[30] G.W. Burdick, M.F. Reid, $4f^n$–$4f^{n-1}5d$ transitions, in: K.A. Gschneidner Jr., J.-C.G. Bünzli, V.K. Pecharsky (Eds.), Handbook on the Physics and Chemistry of Rare Earths, vol. 37, Elsevier B.V., 2007, p. 80.
[31] E. Antic-Fidancev, J. Alloys Compd. 300–301 (300) (2000) 2.
[32] M. Yin, C. Duan, W. Zhang, L. Lou, S. Xia, J.-C. Krupa, J. Appl. Phys. 86 (1999) 3751–3757.
[33] K. Jang, K. Lee, H. Kim, D.S. Shin, S. Park, J. Phys. Soc. Jpn. 68 (1999) 2825–2828.
[34] Z. Qi, C. Shi, W.W. Zhang, W.P. Zhang, T. Hu, Appl. Phys. Lett. 81 (2002) 2857–2859.
[35] W.J.L. Oomen, A.M.A. van Dongen, J. Non-Cryst. Solids 111 (1989) 205–213.
[36] S.A. Wade, S.F. Collins, G.W. Baxter, J. Appl. Phys. 94 (2003) 4743–4756.
[37] S.F. Collins, G.W. Baxter, S.A. Wade, T. Sun, K.T.V. Grattan, Z.Y. Zhang, A.W. Palmer, J. Appl. Phys. 84 (1998) 4649–4654.
[38] R. Abbasova, S. Visintin, V. Sergo, J. Mater. Sci. 40 (2005) 1593–1597.
[39] D. Banejee, H. Rho, H.E. Jackson, R.N. Singh, Compos. Sci. Technol. 61 (2001) 1639–1647.
[40] D.M. Lipkin, D.R. Clarke, Oxid. Met. 45 (1996) 267–280.